Modelling low energy electron interactions for biomedical uses of radiation

Journal of Physics: Conference Series **194** (2009) 012028 doi:10.1088/1742-6596/194/1/012028

Modelling low energy electron interactions for biomedical uses of radiation

M Fuss[1], A Muñoz[2], J C Oller[2], F Blanco[3], P Limão-Vieira[4], C Huerga[5], M Téllez[5], M J Hubin-Fraskin[6], K Nixon[7], M Brunger[7] and G García[1, 8]

[1] Instituto de Física Fundamental, Consejo Superior de Investigaciones Científicas (CSIC), Serrano 113-bis, 28006 Madrid, Spain
[2] Centro de Investigaciones Energéticas, Medioambientales y Tecnológicas (CIEMAT), Avenida Complutense 22, 28040 Madrid, Spain
[3] Departamento de Física Atómica, Molecular y Nuclear, Universidad Complutense de Madrid, Avenida Complutense s.n., 28040 Madrid, Spain
[4] Departamento de Física, Universidade Nova de Lisboa, 2829-516 Caparica, Portugal
[5] Hospital Universitario La Paz, paseo de la Castellana 261, 28046 Madrid, Spain
[6] Department of Chemistry, University of Liège, 4000 Liège 1, Belgium
[7] School of Chemistry, Physics and Earth Sciences, Flinders University, GPO Box 2100, Adelaide, SA 5001, Australia
[8] Departamento de Física de los Materiales, Facultad de Ciencias, Universidad Nacional de Educación a Distancia (UNED), Senda del Rey 9, 28040 Madrid, Spain

E-mail: g.garcia@imaff.cfmac.csic.es

Abstract. Current radiation based medical applications in the field of radiotherapy, radiodiagnostic and radiation protection require modelling single particle interactions at the molecular level. Due to their relevance in radiation damage to biological systems, special attention should be paid to include the effect of low energy secondary electrons. In this study we present a single track simulation procedure for photons and electrons which is based on reliable experimental and theoretical cross section data and the energy loss distribution functions derived from our experiments. The effect of including secondary electron interactions in this model will be discussed.

1. Introduction

Specific radiotherapy techniques are demanding an increasing level of detail to the energy deposition models used for treatment assessments. This is the case of brachytherapy [1-2] and some accelerator based (protons, heavy ions and synchrotron radiation) therapies [3-4] in which irradiated areas are extremely reduced and the absorbed dose in surrounding healthy tissue should be minimized. When molecular details are important, as it is the case with DNA damage studies, spatial resolution should be within the order of magnitude of a nanometre. For this level of description, atomic and molecular properties of the target need to be taken into account. High energy radiation produces abundant secondary electrons which are the main source of the energy transfer map and the radiation damage. Pioneering studies of Huels, Sanche and co-workers [5,6,7] show that even sub-ionising electrons could produce damage, in terms of strand breaks and molecular dissociations, more efficiently than

traditionally considered ways, such as ionisation of the medium. At the nanoscale, it is obvious that conventional radiation detectors based on gas counters are not appropriate devices. New radiation detector developments based on reduced area semiconductors or molecular targeted materials are needed. These reasons support designing radiation interaction models at the molecular level including secondary electron effects.

In this study we present a model which is based on experimental and theoretical electron scattering cross sections as well as on the observed energy loss distribution functions for basic constituents of biological systems, i.e., water, simple hydrocarbons, and DNA subunits.

2. Input Data

Although the main objective of this study is to introduce the effect of the secondary electrons in the above mentioned application, a complete description of these effects requires considering primary high energy particle interactions. In this study we will only treat cases in which these primary particles are photons (with energies around 100 keV) or high energy (up to 4 MeV) electrons. To define trajectories of both primary and secondary particles we need interaction probabilities over a broad energy range for all accessible processes as well as the corresponding energy loss patterns. Complete sets of input data are obtained by combining theoretical and experimental data available in the literature with our own electron scattering and energy loss measurements, and calculation with high energy extrapolations based on the Born-Bethe approximation [8,9]. A description of data requirements classified by particle and energy range can be summarised as follows:

2.1. Photon interaction data

Photon interaction cross section data, both differential and integral, used in this study have been taken from the literature [10] for incident energies from 1 to 100 keV. Integral data for the main processes in water are shown in figure 1 in terms of partial mass attenuation coefficients.

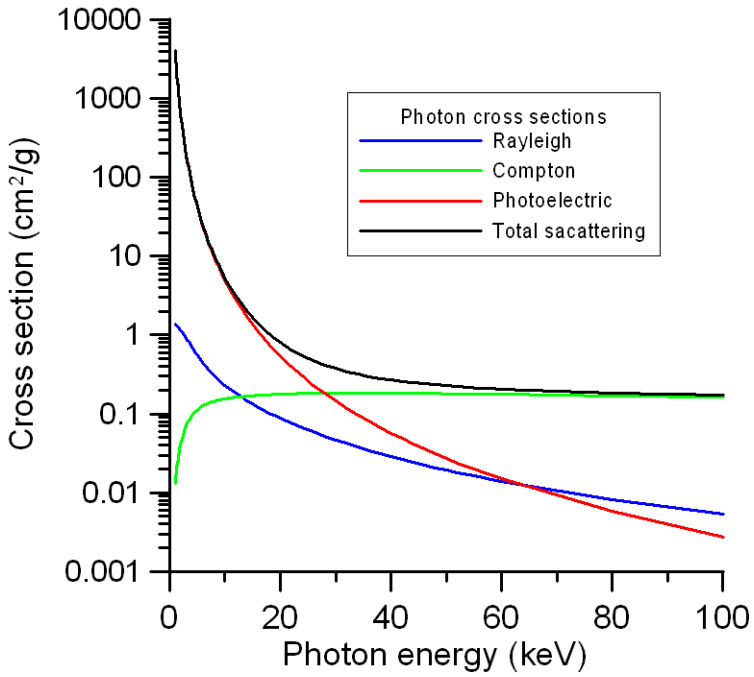

Figure 1. Integral photon scattering cross section (mass attenuation coefficients) in H_2O for incident energies up to 100 keV given in Ref [10].

As may be seen from this figure, in the photon energy range considered here (10-100 keV) Compton scattering and photoelectric interactions are dominant, therefore the photons are considered as a high energy secondary electron source. While photon tracks will be simulated in the same way as in other available codes [11,12,13,14,15] (PENELOPE, GEANT-4), once a secondary electron is generated its evolution will be followed by our simulation programme which is described in section 3.1.

2.2. Electron interaction data

To obtain a reliable complete set of electron interaction data with basic molecules of relevance for the mentioned applications, as it is the case of water and methane, is one of the first objectives of this study. In these applications, electrons can appear as primary radiation or can be generated as secondary electrons by photons and primary electrons. Whatever the electron's origin, when a collision event takes place, an amount of the incident energy can be transferred to the target as internal energy (inelastic scattering) or not, simply transferring linear momentum (elastic scattering). In both cases, the energy and direction of emerging particles need to be known. In other words, we need to know both differential and integral cross sections for all the possible collisions, elastic and inelastic, that can take place in the considered energy range. Another important parameter to model energy deposition in the medium is the energy loss per single event.

Consequently, interaction cross section data, both differential and integral, are needed from very low energies, close to zero, up to the maximum energy of beta emitter radioactive sources, typically some MeV. In order to organise the data requirements, we have divided this wide range into three minor energy regions: the lowest energy region will extend from 0 to 50 eV, the intermediate energy range from 50 to 10000 eV and we will consider the high energy domain above 10 keV, up to few MeV. This classification is based on the specific theoretical and experimental methods that can be used in each interval to get reasonably accurate cross section data. Going from high to low energies, we will give a brief description of these methods:

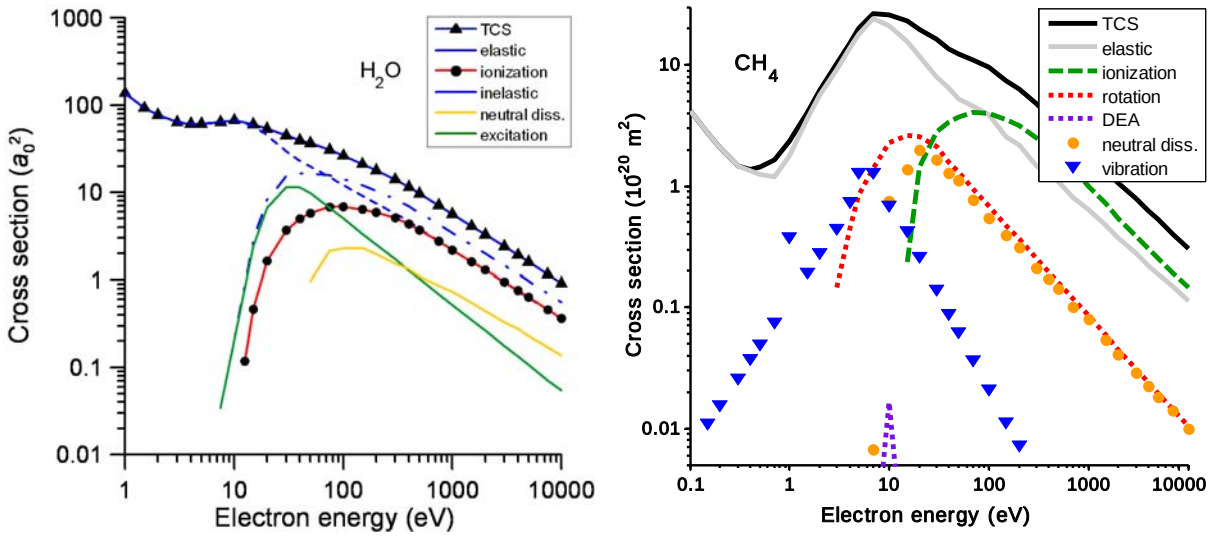

Figure 2. Integral cross sections used for simulations in water (left panel) and methane (right panel).

2.2.1. *High energies, above 10 keV.* Most biomolecular systems contain only relatively light atoms, H, C, N, and O. In general, for energies above 10 keV, electrons see these systems as a combination of atoms with the interaction with each single atom rather well described by the first Born approximation and the Born-Bethe theory [8,9]. As far as integral cross sections for constituent atoms are concerned,

relativistic formulae given in [8,9] can provide any required data, including density effects when they are needed.

2.2.2. *Intermediate energy region, from 50 eV to10 keV.* For intermediate energies, measurements of the total (TCS) and ionization cross sections and of the electron energy loss (EEL) spectra [16,17] were conducted. TCS were measured by means of a transmission beam technique which is described in detail in [18]. By replacing the scattering chamber with an effusive molecular beam, EEL spectra could be measured at different angles by rotating the electron gun with respect to the spectrometer. Ionization cross sections in this energy range were derived from the currents arising from the synchronized extraction of electrons and ions.

Complementary calculations of integral and differential cross sections were done with an optical potential method in the independent atom approximation [19] using screening corrections [20] in order to account for the overlapping of the constituent atoms. This procedure was recently extended for the treatment of large molecules [21] so that applications involving biological macro-molecules can be addressed in the future. After verifying the excellent agreement between theoretical and experimental total cross sections [16,22], remaining inelastic cross sections and differential elastic cross sections were obtained from the calculations in the intermediate energy range. To illustrate this procedure, a set of integral cross section data in this energy range for water and methane is shown in figure 2.

2.2.3. *Low energies, below 50 eV. At* low energies, in view of unresolved discrepancies between experimental and theoretical data, input data was taken from experimental sources, deemed to resemble the conditions of the applications presented here more closely. TCS recently measured by our group [16] as well as the ones published by Čurík *et al.* [23] and Szmytkowski [24] were used as the input data for simulations. Other (elastic and inelastic) integral cross sections were determined by comparing and combining data available in the literature ([25,26,22], see also ref. [27]) with our calculations. Angular distribution functions were taken from the calculations and available experimental data [28], by representing the differential cross sections obtained as functions of the momentum transfer to the medium and thereby considering the incident electron's energy loss in the case of inelastic collisions. Experimental energy loss distributions given in [26] were used.

3. Radiation track modelling

The computational model used for our radiation track simulations has been especially designed to include accurate physical models of all the radiation–matter interactions of interest, even at low energies (≈ 1 eV). Whereas for photon interactions, standard libraries such as [10] achieve satisfactory results, electron interactions are treated by entirely new routines developed by our group. As a result, the simulations yield detailed output including information about the exact type of interaction produced at each point, the secondary electrons generated, and three-dimensional distributions of energy deposition, in addition to penetration depth, beam dispersion and attenuation, etc.

3.1. Monte Carlo simulation

The Monte Carlo code used for our simulations [29,30,20] is a C++ programme based on the GEANT-4 code [14] for making geometrical and materials definitions, sampling processes, and generating graphical output, as well as for photon physics using the built-in toolkit and standard libraries [10]. However, for calculating electron interactions, the GEANT-4 procedures are replaced by our own elastic and inelastic scattering routines using a new modelling approach. Primary and secondary electrons (whether generated by incident photons or by other electrons) are treated identically and are fully simulated until losing all of their energy.

For an incoming electron, the free path in the medium of interest is first sampled according to the total cross section corresponding to its energy. Once the location of the next collision is thus defined, partial cross sections determine whether an elastic or inelastic event is to take place and call the appropriate interaction routine. For elastic collisions, since no energy is deposited in the medium, the

programme simply needs to sample the outgoing particle's angle according to the distribution established by the differential cross sections. In the case of inelastic collisions, different subprocesses (weighted with the corresponding integral cross section's value) handle the different types of interactions that are accessible depending on the electron's energy, such as ionization, vibrational or rotational excitation, neutral dissociation, electronic excitation, or dissociative electron attachment.

First, the energy loss is determined as a fixed value (in the case of rotational or vibrational excitation) or from the electron energy loss distributions (for all other inelastic channels). Subsequently, the electron's outgoing direction is sampled using the angular distribution expressed as a function of momentum transfer and considering the before mentioned energy loss. If an ionization has taken place, a secondary electron is automatically generated and enters the simulation process with the energy lost by the primary electron less the ionization energy, moving with the linear momentum transferred by the primary particle to the medium, and in the direction obtained when applying the momentum conservation law. Finally, the interaction event is terminated and the primary electron and any secondary electrons generated are ready to enter the next collision.

3.2. Results

Using the radiation–matter interaction model described above, different situations of interest in biomedical applications or radiation detector physics have been addressed. An example for a monochromatic photon beam absorbed in water, a typical situation in certain external beam radiotherapies, is shown in figure 3. In the left panel, the distribution of photoelectric effect, Compton scattering, and Rayleigh scattering events (red, green, and blue dots, respectively) is shown (pair production is energetically not accessible in the conditions of this simulation). The right panel shows the secondary electrons generated in a detail view.

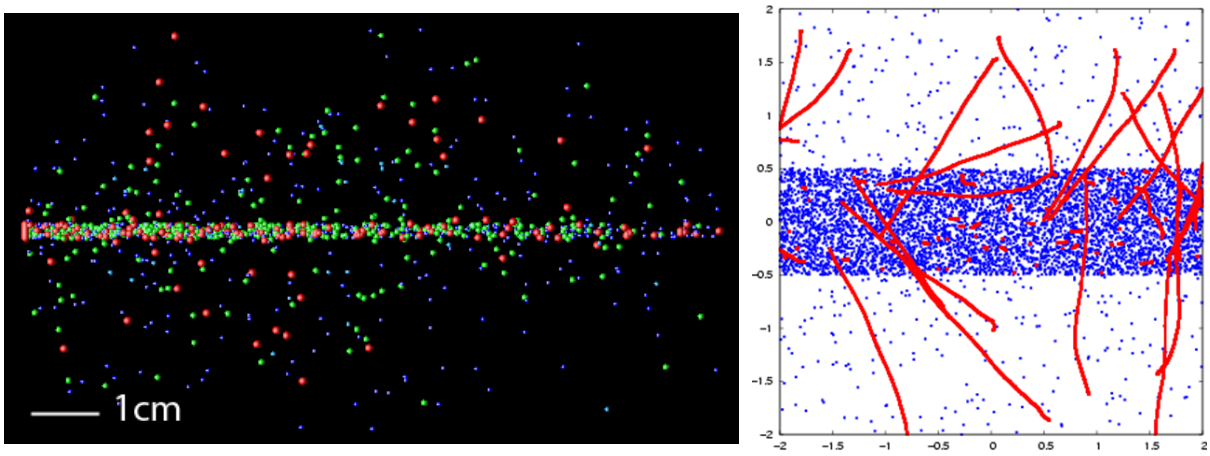

Figure 3. Photons with an initial energy of 60 keV traversing liquid water. Left panel: The different kinds of interactions produced are depicted by the following colours: red – photoelectric effect; green – Compton scattering; blue – Rayleigh scattering. Right panel: Detail (axes in mm). Photons are here shown in blue, while the tracks of secondary electrons are coloured red.

The photon and electron emission spectra of a ^{106}Ru source were employed to simulate plaque brachytherapy of the eye, which is a state-of-the-art treatment for uveal melanoma and other cancers affecting the eyeball. For this application, a valid approximation is obtained by using liquid water to model the eye. The resulting radiation tracks in a three-dimensional representation and the energy deposition as a function of depth in the eye can be seen in figures 4 and 5, respectively.

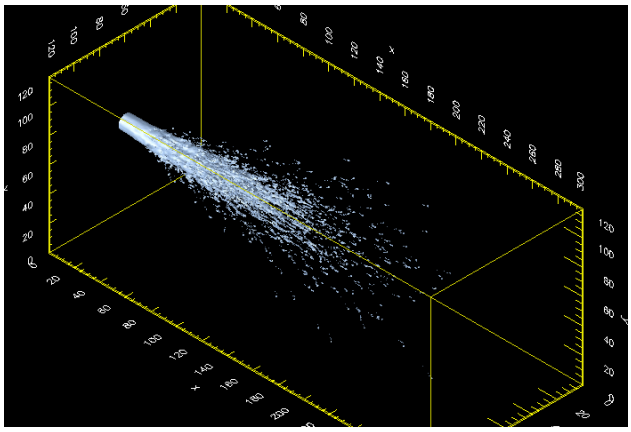

Figure 4. 3D plot of the photon and electron tracks emerging from a ^{106}Ru plaque used for radiotherapy of the eye (the surrounding medium is water).

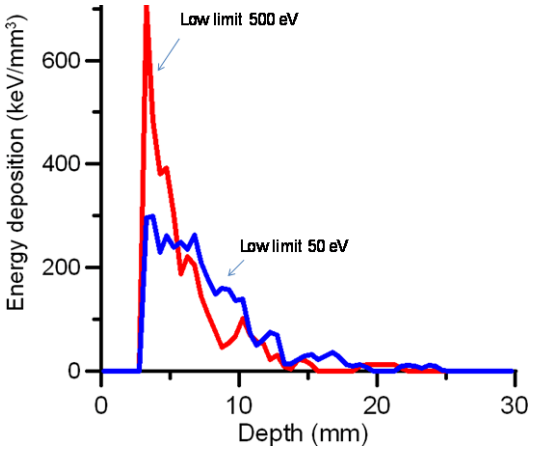

Figure 5. Energy deposition in the eye during ^{106}Ru brachytherapy as a function of depth for different lower limits of electron modelling.

When comparing the energy deposition profile obtained with that provided by other widely-used Monte Carlo codes [e.g. 11], good agreement between the predicted penetration depth can be observed. However, the curve shape exhibits significant differences that can be clearly attributed to the lower energy limit until which electrons are followed in each model (see figure 5). These discrepancies underline the importance of the detailed and physically accurate modelling of low-energy electrons – often lacking in similar Monte Carlo programmes – that is achieved by the simulation here presented.

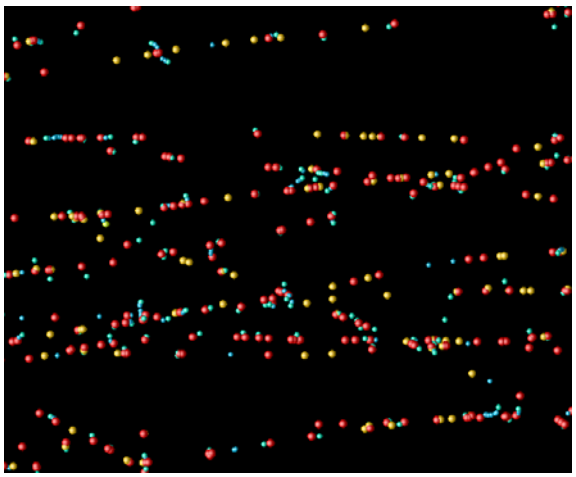

Figure 6. Detail (~1mm) of a jet of electrons traversing CH_4 in the gas phase at a pressure of 0.5 atm (initial energy 10 keV, remaining energy 8–9 keV). The different possible interactions in this case are: • ionization; • neutral dissociation; • vibrational excitation; • rotational excitation; • dissociative e^- attachment (DEA); and elastic collision (not shown for clarity).

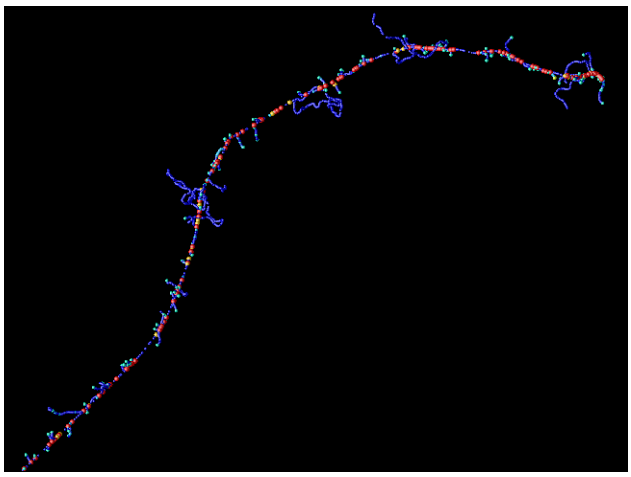

Figure 7. Final part of the trajectory of a single primary electron (same conditions as in figure 6). Colours are used as in figure 6, with elastic collisions now included (•). As can be seen, the secondary electrons produced by ionization events are also followed by the simulation, providing more detailed information about energy carried away from the incident electron's track.

Methane is often used as a filling gas, either pure or in mixtures (e.g., CH_4-based tissue equivalent materials) for radiation detectors such as proportional counters or ionization chambers. Adequate models of electron interactions in methane are therefore critical for numerous dosimetric applications. The trajectories obtained by applying our simulation to electrons interacting with methane can be seen in figures 6 (detail view of many electrons shortly after the start) and 7 (curved part of a single electron track near the end).

In contrast to methane-based tissue equivalent materials [31], almost no data is currently available for the stopping power of electrons in pure methane, and reference values provided by the NIST [32] are based on the first Born approximation that cannot be assumed at low energies. In fact, the mass stopping power calculated by means of our interaction model (see figure 8) shows large discrepancies of the order of 50% with NIST values in the overlapping energy region, suggesting that the mentioned approximation is not valid until higher energies.

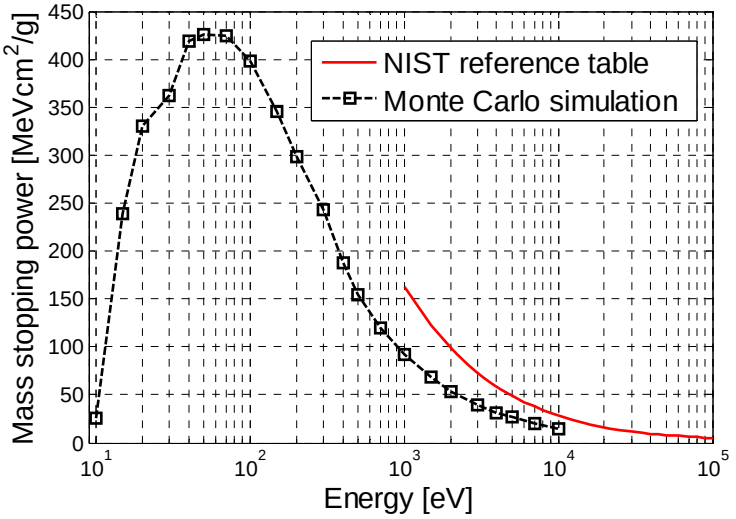

Figure 8. Calculated mass stopping power for electrons in CH_4.

4. Conclusions

In this study, we have presented an interaction model for photon and electron radiation that has been applied to studies in different materials of current interest in biomedicine and radiation detection. Our simulation uses carefully selected mostly experimental input data and specially developed scattering routines in order to provide a detailed, realistic description of the collisional processes taking place at the molecular level. Special attention is paid to the correct inclusion of (primary as well as secondary) low-energy electrons, enhancing for this reason the reliability of the results obtained.

Acknowledgements

This study has been partially supported by the following research projects and institutions: Ministerio de Educación y Ciencia (Plan Nacional de Física, Project FIS2006-00702), Consejo de Seguridad Nuclear (CSN), European Science Foundation (COST Action P9 and EIPAM Project), Acciones Integradas Hispano-Portuguesas (Project HP2006-0042). Hospital Universitario La Paz (Comunidad de Madrid). We acknowledge technical support from the Spanish National Institute for Fusion Research of CIEMAT.

References

[1] Georgopoulos M, Zehetmayer M, Ruhswurm I, Toma-Bstaending S, Ségur-Eltz N, Sacu S and Menapace R 2003 *Ophthalmologica* **217** 315–9

[2] Fuller D B, Koziol J A and Feng A C 2004 *Brachytherapy* **3** 10–9
[3] Slatkin D N, Spanne P, Dilmanian F A and Sandborg M 1992 *Med. Phys.* **19** 1395–400
[4] Gemmel A, Hasch B, Ellerbrock M, Ewyrather W K and Krämer M 2008 *Phys. Med. Biol.***53** 6991–7012
[5] Boudaïffa B, Cloutier P, Hunting D, Huels M A and Sanche L 2000 *Science* **287** 1658–60
[6] Boudaïffa B, Cloutier P, Hunting D, Huels M A and Sanche L 2002 *Radiat. Res.* **157** 227–34
[7] Huels M A, Boudaïffa B, Cloutier P, Hunting D and Sanche L 2003.*J. Am. Chem. Soc.* **125** 4467–77
[8] Inokuti M and McDowell M R C 1975 *J. Phys.* B **7**, 2382–95
[9] Inokuti M 1971 *Rev. Mod. Phys.* **43**, 297–347
[10] Cullen D, Hubbell J H and Kissel L 1997 *EPDL1997: The Evaluated Photon Data Library, '97 Version*, UCRL–50400, vol. 6
[11] Baró J, Sempau J, Fernández-Varea J M and Salvat F 1995 *Nucl. Instrum. Meth.* B **100** 31–46
[12] Sempau J, Acosta E, Baro J, Fernández-Varea J M and Salvat F 1997 *Nucl. Instrum. Meth.* B **132** 377–90
[13] Sempau J, Fernández-Varea J M, Acosta E and Salvat F 2003 *Nucl. Instrum. Meth.* B **207** 107–23
[14] Agostinelli S *et al.* 2003 *Nucl. Instrum. Meth.* A **506** 250
[15] Ivanchenko V N and For Geant4 Collaboration 2004 *Nucl. Instrum. Meth.* A **525** 402–5
[16] Muñoz A, Oller J C, Blanco F, Gorfinkiel J D, Limão-Vieira P and García G 2007 *Phys. Rev.* A **76** 052707
[17] García G and Manero F 1998 *Phys. Rev.* A **57** 1069–73
[18] Limão-Vieira P, Blanco F, Oller J C, Muñoz A, Pérez J M, Vinodkumar M, García G and Mason N J 2005 *Phys. Rev.* A **71** 032720
[19] Blanco F and García G 2003 *Phys. Lett.* A **295** 317
Blanco F and García G 2003 *Phys. Rev.* A **67** 027701
[20] Muñoz A, Blanco F, Oller J C, Pérez J M and García G 2007 *Adv. Quant. Chem.* **52** 21-57
[21] Blanco F and García G 2009 *J. Phys.* B **42** 145203
[22] Karwasz G P, Brusa R S and Zecca A 2001 *Riv. Nuovo Cimento* **24** 12–21
[23] Čurík R, Ziesel J P, Jones N C, Field T A and Field D 2006 *Phys. Rev. Lett.* **97** 123202
[24] Szmytkowski C 1987 *Chem. Phys. Lett.* **136** 363
[25] Itikawa Y and Mason N J 2005 *J. Phys. Chem. Ref. Data* **34** 1
[26] Thorn P A, Brunger M J, Teubner P J O, Diakomichalis N, Maddern T, Bolorizadeh M A, Newell W R, Kato H, Hoshino M, Tanaka H, Cho H and Kim Y-K 2007 *J. Chem. Phys.* **126** 064306
Brunger M J, Thorn P A, Campbell L, Diakomichalis N, Kato H, Kawahara H, Hoshino M, Tanaka H and Kim Y-K 2008 *Int. J. Mass Spectrom.* **271** 80
Thorn P A, Brunger M J, Kato H, Hoshino M and Tanaka H 2007 *J. Phys.* B **40** 697–708
[27] Muñoz A, Blanco F, García G, Thorn P A, Brunger M J, Sullivan J P and Buckman S J 2008 *Int. J. Mass Spectrom.* **277** 175–9
[28] Boesten L and Tanaka H 1991 *J. Phys.* B **24** 821–32
Cho H, Park Y S, Castro E A, de Souza G L C, Iga I, Machado L E, Brescansin L M and Lee M-T 2008 *J. Phys.* B **41** 045203
[29] Muñoz A, Pérez J M, García G and Blanco F 2005 *Nucl. Instrum. Meth.* A **536** 176
[30] Muñoz A, Williart A, Pérez J M, Blanco F and García G 2004 *J. Appl. Phys.* **95** 5865
[31] Waibel E and Grosswendt E 1992 *Phys. Med. Biol.* **37** 1127–45
Oller J C, Muñoz A, Pérez J M, Blanco F, Limão-Vieira P and García G 2006 *Chem. Phys. Lett.* **421** 439–43
[32] National Institute of Standards and Technology 2009 *Stopping-power and range tables for electrons*, available from: http://physics.nist.gov/PhysRefData/Star/Text/ESTAR.html